2024 IEEE 63rd Conference on Decision and Control (CDC)
December 16-19, 2024. MiCo, Milan, Italy

Encirclement Control for PDE-Based Leader-Follower Multi-Agent Systems with Targets in a Sphere: Part 1 – Target Enclosing

Milad Hasanzadeh[1] and Shu-Xia Tang[1]

2024 IEEE 63rd Conference on Decision and Control (CDC) | 979-8-3503-1633-9/24/$31.00 ©2024 IEEE | DOI: 10.1109/CDC56724.2024.10885953

***Abstract*— This paper introduces an innovative target-enclosing control designed for parabolic Partial Differential Equation (PDE)-based multi-agent systems, emphasizing multi-step control within the domain and boundaries consisting of 2 parts. Diverging from prior research, our study delves into a three-dimensional enclosing control and employs PDE control for the system. At part 1, the targets in focus are dynamic, constrained to movement within a three-dimensional neighborhood. Our approach involves overcoming multi-step challenges by utilizing backstepping control for boundary agents acting as leaders. The three consecutive challenges involve prompting agent movement to reach to targets, reforming their formation to establish an appropriate distance for surrounding all targets, and finally achieving a successful enclosing in a distributed manner. Upon a successful target-enclosing in part 1, which can be treated as a standalone result, the next steps are to keep encircling them in part 2. Stability analysis of the closed-loop system is conducted using the Lyapunov technique. Finally, we conduct simulation to evaluate the effectiveness of our proposed methodology.**

***Index Terms*— Multi-Agent Systems, Encirclement Control, PDE control, Boundary control, Finite difference method.**

I. Introduction

Cooperative formation control aims to guide a group of autonomous agents to achieve predefined target formations through decentralized decision-making based on local information rather than relying on global data [1]. Numerous studies exist on MAS formation control, often relying on conventional discrete ordinary differential equation (ODE) models. For instance, [2] examines the feasibility of formations for MASs, while [3] delves into finite-time formation control. Additionally, [4] investigates formation control for time-delayed second-order MASs, and [5] introduces time-varying formation tracking control for high-order nonlinear multi-agent systems. Advancements in modeling large-scale multi-agent systems have shifted towards a continuum-based approach, primarily utilizing PDE models as pioneered by [6]–[8]. In [9], formation control of MASs is investigated using two 2-D reaction-advection-diffusion PDEs to model the system's dynamics. These PDEs represent the positions of agents, where the first one is complex-valued. The second PDE is real-valued and describes height. [10] recently investigated the deployment of agents distributed on a disk-shaped grid onto three-dimensional profiles using backstepping approach.

Target-enclosing stands as a prominent MAS application, involving a group of agents working collectively to surround a target entity and shaping a formation around it, as seen in [11]. [12] explores target encirclement using a cyclic pursuit strategy, while [13] investigates it for MASs with a second-order model. Notably, all these studies in target enclosing predominantly rely on ODE models, whereas our focus lies on employing a PDE-based continuum model for our large-scale MAS.

Encirclement, a significant MAS application, involves a collective effort of agents to enclose a target entity, whether it's a moving intruder or a stationary object, as discussed in [14], [15]. This strategy encompasses target enclosing, followed by a rotation approach to maintain the encirclement and safeguard the targets. In this part of our paper, we delve into target enclosing for parabolic PDE-based MASs, employing a leader-follower approach. In the subsequent part, we focus on the rotating encirclement strategy and formation adjustments.

- To the best of the author's knowledge, this study presents the first introduction of target-enclosing control specifically designed for PDE-based multi-agent systems in a 3-dimensional space. The emphasis lies on multi-step control strategies applied within boundaries.
- Compared with [9] which focus on the PDE-based multi-agent formation control, this paper introduces several advancements. One notable contribution lies in PDE-based **target-enclosing control** where both formation control and **translation** control design has been used to enclose targets based on a multi-step control design.
- Compared with works in [12], [13] which focus on the target-enclosing control for ODE-based models on 2D surface, this paper differentiate itself by **PDE-based model** for multi-agent systems on 3D coordinate where **large-scale MAS** is considered here.

II. Problem Statement

Encirclement control involves designing a controller for $n \times m$ agents to surround p targets, ensuring agents encircle and rotate around the targets without collisions as shown in Fig. 1. We define the targets as $\Phi = \{1, 2, ..., p\}$ and the agents as $\Psi = \{(i, j) : i \in \{1, ..., n\}, j \in \{1, ..., m\}\}$. To prevent collisions, we use a PDE system with specific boundary conditions, assigning unique IDs to agents to maintain distinct positions in cylindrical space. To prevent collision among agents with targets, the encirclement process is divided into four steps, each addressing a specific challenge. Once the control in the current step addresses the challenge, the subsequent control will be applied to address the next

[1]Milad Hasanzadeh and Shu-Xia Tang (corresponding author) are with the Department of Mechanical Engineering, Texas Tech University, Texas, USA m.hasanzadeh@ttu.edu, shuxia.tang@ttu.edu.

Authorized licensed use limited to: Texas Tech University. Downloaded on March 19,2025 at 18:55:59 UTC from IEEE Xplore. Restrictions apply.

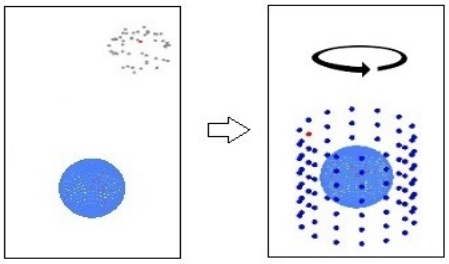

Fig. 1: Gray spheres represent agents in their initial positions, while blue spheres represent their intended positions during encirclement. Additionally, the larger cyan sphere indicates the space occupied by the targets.

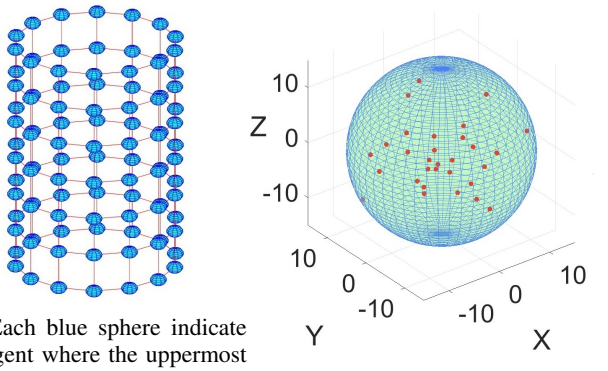

(a) Each blue sphere indicate an agent where the uppermost and lowermost layers consist of leaders.

(b) Targets are pointed with red spheres inside the light green sphere.

Fig. 2: (a) Agents' communication topology, (b) The sphere of targets.

challenge accordingly. In total, four steps of successive challenges are addressed to fulfill the paper's objective. Let $\Xi = \{1, 2, 3, 4\}$ represent the set of all steps. Steps one to three will be addressed in the concept of boundary control and the last step will be treated as in-domain control in [16]. The first three steps will be investigated in this part and the fourth step is investigated in the second part.

A. Targets' Profile

Throughout the paper, the position of target $i \in \Phi$ in 3D space along the coordinate axes (x, y, z) is denoted as $\boldsymbol{w}_i^{\text{ta}}(t) = [x_i^{\text{ta}}(t), y_i^{\text{ta}}(t), z_i^{\text{ta}}(t)]^T$. For simplicity, in the remainder of this paper, we abbreviate $\boldsymbol{w}_i^{\text{ta}}(t)$ as $\boldsymbol{w}_i^{\text{ta}}$. The dynamics of targets are governed by following assumptions.

Assumption 1: $\boldsymbol{w}_i^{\text{ta}}$, $\forall i \in \Phi$, are continuously differentiable and the velocity of targets $\forall t > 0$ is bounded as

$$\|\dot{\boldsymbol{w}}_i^{\text{ta}}\| \leqslant \beta, \tag{1}$$

where β is a positive constant.

Assumption 2: Targets will not collide with each other, that is $\forall t > 0, i, j, i \neq j \in \Phi$,

$$\boldsymbol{w}_j^{\text{ta}} \neq \boldsymbol{w}_i^{\text{ta}}. \tag{2}$$

Assumption 3: Targets' dynamics are bounded that means the movements of targets are limited within a spherical area that is $\forall i \in \Phi$ we have

$$\sup_{t>0} \|\boldsymbol{w}_i^{\text{ta}}(t) - \boldsymbol{w}^{\star}\| \leqslant r^{\star}, \tag{3}$$

where $\boldsymbol{w}^{\star} = [x^{\star}, y^{\star}, z^{\star}]^T, r^{\star}$ are the center and the radius of the sphere.

Fig. 2b is demonstrating the location of targets in the spherical area described by Assumption 3.

B. Agents' Dynamic

A group of $n \times m$ agents navigating in a 3D space along the coordinate axes (x, y, z). n stands for the total number of agents (blue spheres) in each circle of the cylindrical mesh grid shown in Fig. (2a) and m stands for the total number of circles of the cylindrical mesh grid. To streamline the notation, we introduce the complex-valued variable $u = x + jy$ to represent the state components on the (x, y) axes. An indirect topology graph is defined on a cylindrical surface, as shown in Fig. 2a, to determine the neighbor set of each agent.

As the number of agents increases, particularly for large m and n, we consider the agents as a continuum, enabling the mapping of discrete identification (ID) numbers (i, j) of the agents (θ_i, s_j) to coordinates on the cylindrical surface $\Omega = \{(\theta, s) : -\pi \leqslant \theta < \pi, 0 \leqslant s \leqslant 1\}$. This mapping, $(\theta_i, s_j) \to (\theta, s)$, occurs as $m, n \to \infty$. Consequently, the multi-agent systems, operating on a large scale, are effectively modeled as PDE. In this section, we aim to use linear parabolic PDE to describe the collective dynamics of the multi-agent system. Consider the position of agent $(i, j) \in \Psi$ in 3D space is denoted as $u^{\text{ag}}(t, \theta, s)$ along with $z^{\text{ag}}(t, \theta, s)$. Based on the concept of boundary actuation, leaders are selected from agents positioned at the uppermost and lowermost layers of the topology surface shown in Fig. 2a. Based on the [9], the collective dynamics of the agent system is modeled by a system of two reaction–advection–diffusion PDE as

$$u_t^{\text{ag}}(t, \theta, s) = \Delta u^{\text{ag}}(t, \theta, s) + \alpha_1 u_s^{\text{ag}}(t, \theta, s) + \zeta_1 u^{\text{ag}}(t, \theta, s), \tag{4a}$$

$$z_t^{\text{ag}}(t, \theta, s) = \Delta z^{\text{ag}}(t, \theta, s) + \alpha_2 z_s^{\text{ag}}(t, \theta, s) + \zeta_2 z^{\text{ag}}(t, \theta, s), \tag{4b}$$

$$u^{\text{ag}}(t, \theta, 0) = f_1(\theta), \quad u^{\text{ag}}(t, \theta, 1) = g_1(\theta) + U(t, \theta), \tag{4c}$$

$$u^{\text{ag}}(t, -\pi, s) = u^{\text{ag}}(t, \pi, s) \tag{4d}$$

$$z^{\text{ag}}(t, \theta, 0) = f_2(\theta), \quad z^{\text{ag}}(t, \theta, 1) = g_2(\theta) + Z(t, \theta), \tag{4e}$$

$$z^{\text{ag}}(t, -\pi, s) = z^{\text{ag}}(t, \pi, s). \tag{4f}$$

In the context of $(t, \theta, s) \in \mathbb{R}^+ \times \Omega$, where θ and s represent spatial variables and agent IDs on the communication topology, respectively, $u, \alpha_1, \zeta_1 \in \mathbb{C}$ and $z, \alpha_2, \zeta_2 \in \mathbb{R}$. Additionally, $f_1(\theta), g_1(\theta)$ and $f_2(\theta), g_2(\theta)$ denote non-zero and bounded boundary conditions for states u and z, respectively, representing the open-loop formation of leaders. Controllers $U(t, \theta)$ and $Z(t, \theta)$ will be designed for horizontal and vertical coordinates to stabilize the system to certain desired profile. The system represented by (4) will be employed for the first three steps of the main problem, where backstepping control will be utilized to tackle these challenges. Δ denotes

Authorized licensed use limited to: Texas Tech University. Downloaded on March 19,2025 at 18:55:59 UTC from IEEE Xplore. Restrictions apply.

the Laplace operator as in [9]. The steady-state solutions $(\bar{u}^{\mathrm{ag}}(\theta,s),\bar{z}^{\mathrm{ag}}(\theta,s))$ to the system (4) satisfy the following

$$\Delta\bar{u}^{\mathrm{ag}}(\theta,s)+\alpha_1\bar{u}_s^{\mathrm{ag}}(\theta,s)+\zeta_1\bar{u}^{\mathrm{ag}}(\theta,s)=0, \tag{5a}$$
$$\Delta\bar{z}^{\mathrm{ag}}(\theta,s)+\alpha_2\bar{z}_s^{\mathrm{ag}}(\theta,s)+\zeta_2\bar{z}^{\mathrm{ag}}(\theta,s)=0, \tag{5b}$$
$$\bar{u}^{\mathrm{ag}}(\theta,0)=f_1(\theta),\quad \bar{u}^{\mathrm{ag}}(\theta,1)=g_1(\theta), \tag{5c}$$
$$\bar{u}^{\mathrm{ag}}(0,s)=\bar{u}^{\mathrm{ag}}(2\pi,s), \tag{5d}$$
$$\bar{z}^{\mathrm{ag}}(\theta,0)=f_2(\theta),\quad \bar{z}^{\mathrm{ag}}(\theta,1)=g_2(\theta), \tag{5e}$$
$$\bar{z}^{\mathrm{ag}}(0,s)=\bar{z}(2\pi,s). \tag{5f}$$

Let $a=\alpha_1^2-4\zeta_1+4k^2$, the explicit solution of the complex-valued state is

$$\bar{u}^{\mathrm{ag}}(\theta,s)=\begin{cases}\sum\limits_{k=-\infty}^{\infty}\mathrm{e}^{\mathrm{j}k\theta-\frac{1}{2}\alpha_1 s}\left(A_k\mathrm{e}^{\sqrt{a}s}+B_k\mathrm{e}^{-\sqrt{a}s}\right),\\ \qquad\text{if}\quad a>0,\\ \sum\limits_{k=-\infty}^{\infty}\mathrm{e}^{\mathrm{j}k\theta}\left(A_k\mathrm{e}^{-\frac{1}{2}\alpha_1 s}+B_k s\mathrm{e}^{-\frac{1}{2}\alpha_1 s}\right),\\ \qquad\text{if}\quad a=0,\\ \sum\limits_{k=-\infty}^{\infty}\mathrm{e}^{\mathrm{j}k\theta-\frac{1}{2}\alpha_1 s}\left(A_k\cos\left(\frac{1}{2}\sqrt{-a}s\right)\right.\\ \left.+B_k\sin\left(\frac{1}{2}\sqrt{-a}s\right)\right),\quad\text{if}\quad a<0,\end{cases} \tag{6}$$

where A_k and B_k are constants determined by the boundary conditions given in equations (5c) and (5d). The equilibrium $\bar{z}^{\mathrm{ag}}(\theta,s)$ is determined in a similar manner and the steady-state solution at each step will be indexed by $i\in\Xi$ as $\bar{u}^{\mathrm{ag}}(\theta,s)$ and $\bar{z}^{\mathrm{ag}}(\theta,s)$.

The desired geometric center of the system at each step will be defined as $(u_i^{\diamond},z_i^{\diamond}),\forall i\in\Xi$ where we can define the desired profile of agents $\forall i\in\Xi$ as

$$\tilde{u}_i^{\mathrm{ag}}(\theta,s)=u_i^{\diamond}+\bar{u}_i^{\mathrm{ag}}(\theta,s),\tilde{z}_i^{\mathrm{ag}}(\theta,s)=z_i^{\diamond}+\bar{z}_i^{\mathrm{ag}}(\theta,s). \tag{7}$$

The objective in each step is to design $U(t,\theta)$ and $Z(t,\theta)$ such that $(u^{\mathrm{ag}}(t,\theta,s),z^{\mathrm{ag}}(t,\theta,s))\rightarrow(\tilde{u}_i^{\mathrm{ag}}(\theta,s),\tilde{z}_i^{\mathrm{ag}}(\theta,s))$. Consequently, the controllers in each step will be denoted as $U_i(t,\theta)$ and $Z_i(t,\theta)$. Let the error signals be defined as

$$u_i^{\mathrm{er}}(t,\theta,s)=u^{\mathrm{ag}}(t,\theta,s)-\tilde{u}_i^{\mathrm{ag}}(\theta,s), \tag{8}$$
$$z_i^{\mathrm{er}}(t,\theta,s)=z^{\mathrm{ag}}(t,\theta,s)-\tilde{z}_i^{\mathrm{ag}}(\theta,s), \tag{9}$$

then the error dynamics for the system modeled by (4) are

$$\begin{aligned}u_{i_t}^{\mathrm{er}}(t,\theta,s)&=\Delta u_i^{\mathrm{er}}(t,\theta,s)+\alpha_1 u_{i_s}^{\mathrm{er}}(t,\theta,s)+\zeta_1 u_i^{\mathrm{er}}(t,\theta,s)\\&\quad+\Delta\tilde{u}_i^{\mathrm{ag}}(\theta,s)+\alpha_1\tilde{u}_{i_s}^{\mathrm{ag}}(\theta,s)+\zeta_1\tilde{u}_i^{\mathrm{ag}}(\theta,s)\\&\quad-\tilde{u}_{i_t}^{\mathrm{ag}}(\theta,s),\end{aligned} \tag{10a}$$
$$\begin{aligned}z_{i_t}^{\mathrm{er}}(t,\theta,s)&=\Delta z_i^{\mathrm{er}}(t,\theta,s)+\alpha_2 z_{i_s}^{\mathrm{er}}(t,\theta,s)+\zeta_2 z_i^{\mathrm{er}}(t,\theta,s)\\&\quad+\Delta\tilde{z}_i^{\mathrm{ag}}(\theta,s)+\alpha_2\tilde{z}_{i_s}^{\mathrm{ag}}(\theta,s)+\zeta_2\tilde{z}_i^{\mathrm{ag}}(\theta,s)\\&\quad-\tilde{z}_{i_t}^{\mathrm{ag}}(\theta,s),\end{aligned} \tag{10b}$$
$$u_i^{\mathrm{er}}(t,\theta,0)=0,\quad u_i^{\mathrm{er}}(t,\theta,1)=U_i(t,\theta), \tag{10c}$$
$$u_i^{\mathrm{er}}(t,0,s)=u_i^{\mathrm{er}}(t,2\pi,s) \tag{10d}$$
$$z_i^{\mathrm{er}}(t,\theta,0)=0,\quad z_i^{\mathrm{er}}(t,\theta,1)=Z_i(t,\theta), \tag{10e}$$
$$z_i^{\mathrm{er}}(t,0,s)=z_i^{\mathrm{er}}(t,2\pi,s). \tag{10f}$$

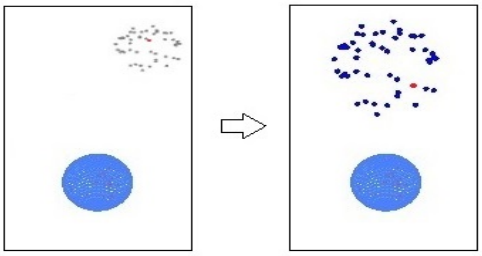

Fig. 3: Translation of agents. Gray spheres represent agents in their initial positions, while blue spheres represent their intended positions at this step. Additionally, the larger cyan sphere indicates the space occupied by the targets.

III. Target-enclosing

A. Step 1: Translation

In this section, the aim is prompting agents' movement to reach to the top side of targets, more specifically we want agents to get close to targets at the upper side of them with avoiding collision and without any specific formation as shown in Fig. 3.

In order to have no collision among the agents, the following functions must be used in the boundary conditions of the system in (5).

$$f_1(\theta)=e^{j\theta},g_1(\theta)=e^{j\theta},f_2(\theta)=0,g_2(\theta)=1. \tag{11}$$

These functions assign a unique label (θ_i,s_j) to each agent, ensuring distinct positions in the random formation. The formation's shape is irrelevant here. Alternative functions, not limited to equation (11), can be used as long as unique labels are preserved. The desired geometric center is defined as

$$u_1^{\diamond}=x^{\star}+jy^{\star},z_1^{\diamond}=\xi z^{\star}, \tag{12}$$

where, $x^{\star},y^{\star}$, and $z^{\star}$ represent the center of the sphere containing the targets, $\xi>1$ is a positive constant, and j is the imaginary unit. Note that $\bar{u}_1^{\mathrm{ag}}=\bar{z}_1^{\mathrm{ag}}=0$ in this step. Substituting (12) into (7) gives the desired profile at step 1.

$$\tilde{u}_1^{\mathrm{ag}}=x^{\star}+jy^{\star},\tilde{z}_1^{\mathrm{ag}}=\xi z^{\star}. \tag{13}$$

By substituting (13) in the error dynamic (10) we have

$$u_{1_t}^{\mathrm{er}}(t,\theta,s)=\Delta u_1^{\mathrm{er}}(t,\theta,s)+\alpha_1 u_{1_s}^{\mathrm{er}}(t,\theta,s)+\zeta_1 u_1^{\mathrm{er}}(t,\theta,s), \tag{14a}$$
$$u_1^{\mathrm{er}}(t,\theta,0)=0,\quad u_1^{\mathrm{er}}(t,\theta,1)=U_1(t,\theta), \tag{14b}$$
$$u_1^{\mathrm{er}}(t,0,s)=u_1^{\mathrm{er}}(t,2\pi,s) \tag{14c}$$

Considering the so-called gauge transformation in (15)

$$v_1(t,\theta,s)=e^{\frac{1}{2}\alpha_1 s}u_1^{\mathrm{er}}(t,\theta,s), \tag{15}$$

and substituting the transformed system state $v_1(t,\theta,s)$ into the Fourier series transform in (16)

$$v_1(t,\theta,s)=\sum_{n=-\infty}^{\infty}v_{1n}(t,s)\mathrm{e}^{\mathrm{j}n\theta}, \tag{16}$$

$$V_1(t,\theta)=\sum_{n=-\infty}^{\infty}V_{1n}(t)\mathrm{e}^{\mathrm{j}n\theta}, \tag{17}$$

Authorized licensed use limited to: Texas Tech University. Downloaded on March 19,2025 at 18:55:59 UTC from IEEE Xplore. Restrictions apply.

where the coefficients v_{1n} and V_{1n}, for $n \in \mathbb{Z}$, satisfy the inverse Fourier series transform, then the error system modeled by (14) is mapped to the following

$$v_{1nt}(t,s) = v_{1nss}(t,s) - n^2 v_{1n}(t,s) + \lambda_1 v_{1n}(t,s), \quad (18a)$$
$$v_{1n}(t,0) = 0, v_{1n}(t,1) = V_{1n}(t), \quad (18b)$$

where $\lambda_1 := \zeta_1 - \frac{1}{4}\alpha_1^2$. For detailed extraction, refer to [9]. The PDE backstepping method from [17] was used to design the controller $V_{1n}(t)$, transforming system (18) into an exponentially stable system.

$$\omega_{nt}(t,s) = \omega_{nss}(t,s) - n^2 \omega_n(t,s), \quad (19a)$$
$$\omega_n(t,0) = 0, \omega_n(t,1) = 0. \quad (19b)$$

(20) maps the system in (18) to (19) successfully.

$$\omega_n(t,s) = v_{1n}(t,s) - \int_0^s K(s,\tau) v_{1n}(t,\tau) d\tau, \quad (20)$$

where the gain Kernel function $K(s,\tau)$ is designed as

$$K(s,\tau) = -\lambda_1 \tau \frac{\mathrm{I}_1\left[\sqrt{\lambda_1(s^2-\tau^2)}\right]}{\sqrt{\lambda_1(s^2-\tau^2)}}, \quad (21)$$

in which I_1 is the first-order modified Bessel function of the first-kind. Based on the gain Kernel design, the controller $V_{1n}(t)$ is designed and based on that the main controller is

$$U_1(t,\theta) = -\int_0^1 \lambda_1 \tau \frac{\mathrm{I}_1\left[\sqrt{\lambda_1(1-\tau^2)}\right]}{\sqrt{\lambda_1(1-\tau^2)}} \mathrm{e}^{-\frac{1}{2}\alpha_1(1-\tau)} \times u_1^{\mathrm{er}}(t,\theta,\tau) d\tau. \quad (22)$$

Also, in a similar way we have

$$Z_1(t,\theta) = -\int_0^1 \lambda_2 \tau \frac{\mathrm{I}_1\left[\sqrt{\lambda_2(1-\tau^2)}\right]}{\sqrt{\lambda_2(1-\tau^2)}} \mathrm{e}^{-\frac{1}{2}\alpha_2(1-\tau)} \times (z_1^{\mathrm{er}}(t,\theta,\tau)) d\tau, \quad (23)$$

where $\lambda_2 := \zeta_2 - \frac{1}{4}\alpha_2^2$.

Theorem 1: Consider the error dynamic in (4) in conjunction with the control design described by (22). The system state is exponentially convergent to the desired geometric center in the sense of L_2 norm where we have

$$\|u^{\mathrm{ag}}(t,\cdot) - \tilde{u}_1^{\mathrm{ag}}(\cdot)\|_{L^2} \leqslant \nu_1 e^{-\frac{1}{2}t} \|u^{\mathrm{ag}}(0,\cdot) - \tilde{u}_1^{\mathrm{ag}}(\cdot)\|_{L^2}.$$

where ν_1 is a positive constant.

The proof is omitted due to page limitations. The behavior of the second system state, $z^{\mathrm{ag}}(t,\theta,s)$, with control design (23), closely resembles the first system. For $\nu_2 > 0$, we have:

$$\|z^{\mathrm{ag}}(t,\cdot) - \tilde{z}_1^{\mathrm{ag}}(\cdot)\|_{L^2} \leqslant \nu_2 e^{-\frac{1}{2}t} \|z^{\mathrm{ag}}(0,\cdot) - \tilde{z}_1^{\mathrm{ag}}(\cdot)\|_{L^2}.$$

B. Step 2: Formation

In this section, the aim for agents is to adjust a cylindrical formation with a bigger radius compared with the radius of the targets' sphere as shown in Fig. 4.

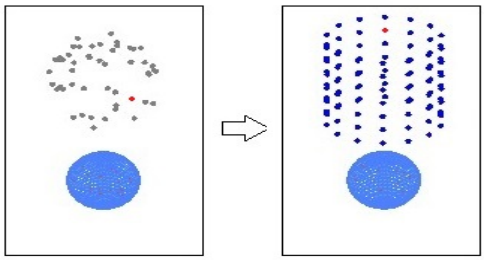

Fig. 4: Formation of agents. Gray spheres represent agents in their initial positions, while blue spheres represent their intended positions at this step.

In order to approach the cylindrical formation, the following functions must be used in the boundary conditions of the system in (5)

$$f_1(\theta) = kr^\star e^{j\theta}, g_1(\theta) = kr^\star e^{j\theta}, f_2(\theta) = 0, g_2(\theta) = 1, \quad (24)$$

where $k > 1$ is a positive constant. These functions assign a unique label (θ_i, s_j) to each agent, ensuring distinct positions in the cylindrical formation. The same functions from (24) are used to calculate the steady-state solution of system (5). The desired geometric center is

$$u_2^\diamond = 0, z_2^\diamond = 0. \quad (25)$$

By substituting the calculated steady state solution (6) and the desired geometric center (25) into the (7), the following desired profile for this step is considered.

$$\tilde{u}_2^{\mathrm{ag}}(\theta,s) = \bar{u}_2^{\mathrm{ag}}(\theta,s), \tilde{z}_1^{\mathrm{ag}}(\theta,s) = \bar{z}_1^{\mathrm{ag}}(\theta,s). \quad (26)$$

By substituting (26) in the error dynamic (10) we have the representative error dynamic as

$$u_{2_t}^{\mathrm{er}}(t,\theta,s) = \Delta u_2^{\mathrm{er}}(t,\theta,s) + \alpha_1 u_{2_s}^{\mathrm{er}}(t,\theta,s) + \zeta_1 u_2^{\mathrm{er}}(t,\theta,s), \quad (27a)$$
$$u_2^{\mathrm{er}}(t,\theta,0) = 0, \quad u_2^{\mathrm{er}}(t,\theta,1) = U_2(t,\theta), \quad (27b)$$
$$u_2^{\mathrm{er}}(t,0,s) = u_2^{\mathrm{er}}(t,2\pi,s) \quad (27c)$$

The following system is presented after applying similar gauge transformation and considering Fourier series coefficients as mentioned in (15), and (16) respectfully

$$v_{2nt}(t,s) = v_{2nss}(t,s) - n^2 v_{2n}(t,s) + \lambda_1 v_{2n}(t,s), \quad (28a)$$
$$v_{2n}(t,0) = 0, v_{2n}(t,1) = V_{2n}(t), \quad (28b)$$

in which v_{2n} and V_{2n}, for $n \in \mathbb{Z}$ are the Fourier transform coefficients. In order to transform system (28) into the exponential stable system (19), the following map is used.

$$\omega_n(t,s) = v_{2n}(t,s) - \int_0^s K(s,\tau) v_{2n}(t,\tau) d\tau, \quad (29)$$

where the gain Kernel function $K(s,\tau)$ is designed in (21). The main controller is

$$U_2(t,\theta) = -\int_0^1 \lambda_1 \tau \frac{\mathrm{I}_1\left[\sqrt{\lambda_1(1-\tau^2)}\right]}{\sqrt{\lambda_1(1-\tau^2)}} \mathrm{e}^{-\frac{1}{2}\alpha_1(1-\tau)} \times u_2^{\mathrm{er}}(t,\theta,\tau) d\tau. \quad (30)$$

Authorized licensed use limited to: Texas Tech University. Downloaded on March 19,2025 at 18:55:59 UTC from IEEE Xplore. Restrictions apply.

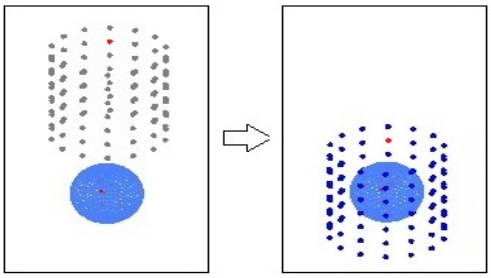

Fig. 5: Target-enclosing by agents. Gray spheres represent agents in their initial positions, while blue spheres represent their intended positions at this step.

Also, in a similar way we have

$$Z_2(t,\theta) = -\int_0^1 \lambda_2 \tau \frac{\mathrm{I}_1\left[\sqrt{\lambda_2\left(1-\tau^2\right)}\right]}{\sqrt{\lambda_2\left(1-\tau^2\right)}} \mathrm{e}^{-\frac{1}{2}\alpha_2(1-\tau)} \times (z_2^{\mathrm{er}}(t,\theta,\tau))d\tau. \tag{31}$$

Theorem 2: Consider the error dynamic in (4) in conjunction with the control design described by (30). The system state is exponentially convergent to the steady state formation in the sense of L_2 norm and we have

$$\|u^{\mathrm{ag}}(t,\cdot) - \tilde{u}_2^{\mathrm{ag}}(\cdot)\|_{L^2} \leqslant \nu_3 e^{-\frac{1}{2}t} \|u^{\mathrm{ag}}(0,\cdot) - \tilde{u}_2^{\mathrm{ag}}(\cdot)\|_{L^2},$$

where ν_3 is a positive constant.
The proof is omitted due to page limitations. Note that the behavior of the second system state, $z^{\mathrm{ag}}(t,\theta,s)$, along with control design (23), closely resembles that of the first system and for $\nu_4 > 0$ we have

$$\|z^{\mathrm{ag}}(t,\cdot) - \tilde{z}_2^{\mathrm{ag}}(\cdot)\|_{L^2} \leqslant \nu_4 e^{-\frac{1}{2}t} \|z^{\mathrm{ag}}(0,\cdot) - \tilde{z}_2^{\mathrm{ag}}(\cdot)\|_{L^2}.$$

C. Step 3: Enclosing

In this section, the aim for agents is to move downside to fully enclose the targets' sphere as shown in Fig. 5 with no change in the formation.

The following functions has been used in the boundary conditions of the system

$$f_1(\theta) = kr^\star e^{j\theta}, g_1(\theta) = kr^\star e^{j\theta}, f_2(\theta) = \eta_1, g_2(\theta) = \eta_2, \tag{32}$$

where $k > 1$ is the positive constant designed in step 2 and $\eta_1, \eta_2 \in \mathbb{Z}$ where $|\eta_1 - \eta_2| = 2r^\star$ and the desired geometric center in this step is

$$u_3^\diamond = x^\star + jy^\star, z_3^\diamond = z^\star. \tag{33}$$

By substituting (33) in the (7) we have the following desired profile at step 3

$$\tilde{u}_3^{\mathrm{ag}} = x^\star + jy^\star, \tilde{z}_3^{\mathrm{ag}} = z^\star. \tag{34}$$

By substituting (34) in the error dynamic (10) we have the representative error dynamic as

$$u_{3_t}^{\mathrm{er}}(t,\theta,s) = \Delta u_3^{\mathrm{er}}(t,\theta,s) + \alpha_1 u_{3_s}^{\mathrm{er}}(t,\theta,s) + \zeta_1 u_3^{\mathrm{er}}(t,\theta,s), \tag{35a}$$

$$u_3^{\mathrm{er}}(t,\theta,0) = 0, \quad u_3^{\mathrm{er}}(t,\theta,1) = U_3(t,\theta), \tag{35b}$$

$$u_3^{\mathrm{er}}(t,0,s) = u_3^{\mathrm{er}}(t,2\pi,s) \tag{35c}$$

Following the same process as explained in step 1 by applying gauge transformation and considering Fourier series coefficients and PDE backstepping method the following main controller are designed

$$U_3(t,\theta) = -\int_0^1 \lambda_1 \tau \frac{\mathrm{I}_1\left[\sqrt{\lambda_1\left(1-\tau^2\right)}\right]}{\sqrt{\lambda_1\left(1-\tau^2\right)}} \mathrm{e}^{-\frac{1}{2}\alpha_1(1-\tau)} \times u_3^{\mathrm{er}}(t,\theta,\tau)d\tau. \tag{36}$$

Also, in a similar way $Z_3(t,\theta)$ is designed as

$$Z_3(t,\theta) = -\int_0^1 \lambda_2 \tau \frac{\mathrm{I}_1\left[\sqrt{\lambda_2\left(1-\tau^2\right)}\right]}{\sqrt{\lambda_2\left(1-\tau^2\right)}} \mathrm{e}^{-\frac{1}{2}\alpha_2(1-\tau)} \times z_3^{\mathrm{er}}(t,\theta,\tau)d\tau. \tag{37}$$

Theorem 3: Consider the error dynamic in (4) in conjunction with the control design described by (36). The system state is exponentially convergent to the desired geometric center in the sense of L_2 norm and we have

$$\|u^{\mathrm{ag}}(t,\cdot) - \tilde{u}_3^{\mathrm{ag}}(\cdot)\|_{L^2} \leqslant \nu_5 e^{-\frac{1}{2}t} \|u^{\mathrm{ag}}(0,\cdot) - \tilde{u}_3^{\mathrm{ag}}(\cdot)\|_{L^2},$$

where ν_5 is a positive constant.
The proof is omitted due to page limitations. Note that the behavior of the second system state, $z^{\mathrm{ag}}(t,\theta,s)$, along with control design (37), closely resembles that of the first system. Step 4 has been investigated in part 2 of this paper.

IV. Simulation

Due to page constraints, the discretization method is explored in the second part of the paper. We consider a group of $p = 20$ dynamic targets enclosed within a sphere centered at $\boldsymbol{w}^\star = [35, 0, 35]^T$ with a radius of $r^\star = 10$. The total number of agents is $n = 10, m = 11$ in total 110 agents. System parameters are set as $\alpha_1 = 0$, $\alpha_2 = 0$, $\zeta_1 = 1$, and $\zeta_2 = 1$. Each step involves a distinct desired formation and/or geometric center. The desired profile for all steps is summarized in Table I in this section. A video that demonstrates all frames of each step is available in [18]. Note

Steps	Geometric center	Formation
translation	$x^\star + jy^\star$,$\xi z^\star$	-
formation	-	$f_1 = g_1 = kr^\star e^{j\theta}, f_2 = 0, g_2 = 1$
enclosing	$x^\star + jy^\star$,$z^\star$	-

TABLE I: Desired profile

that $k = 1.5$ and $\xi = 2$ in this section. Boundary conditions of the system has been chosen for steps 1, 2, and 3 as follows

$$f_1 = g_1 = e^{j\theta}, f_2 = 0, g_2 = 1, \tag{38}$$

$$f_1 = g_1 = kr^\star e^{j\theta}, f_2 = 0, g_2 = 10, \tag{39}$$

$$f_1 = g_1 = kr^\star e^{j\theta}, f_2 = 5, g_2 = -20. \tag{40}$$

Initially, agents' positions are random at all directions using MATLAB command ($>> rand$). Fig. 6 depicts the agents' initial random positions, while Fig. 7 shows their final positions at the top side of targets after the first step. In Fig. 8, agents successfully form the cylindrical formation by

Authorized licensed use limited to: Texas Tech University. Downloaded on March 19,2025 at 18:55:59 UTC from IEEE Xplore. Restrictions apply.

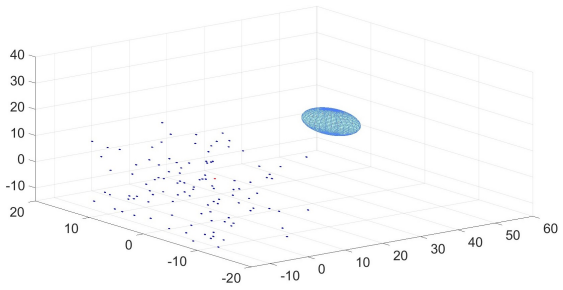

Fig. 6: Agents' initial position at the step 1.

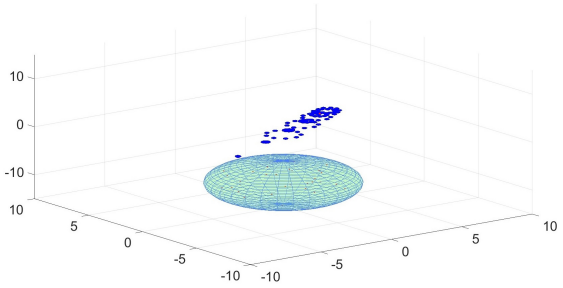

Fig. 7: Agents' final position at the step 1 which is also initial position at the step 2.

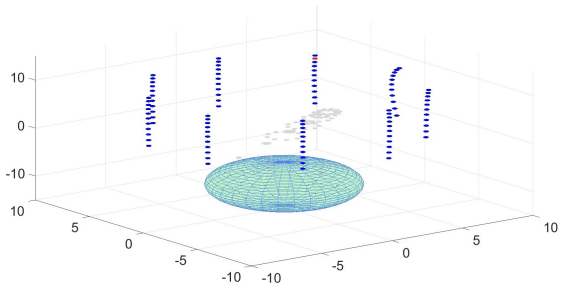

Fig. 8: Agents' final position at the step 2 which is also initial position at the step 3.

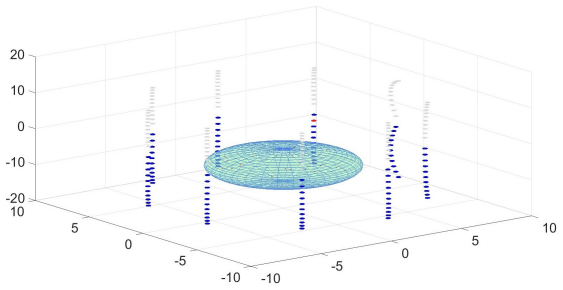

Fig. 9: Agents' final position at the step 3 which is also initial position at the step 4.

the end of step 2, with their initial positions in the second step being their final positions from the previous step (Fig. 7). In Fig. 9, agents' positions at the end of step 3 are shown, where their initial positions in the third step correspond to their final positions from the previous step (Fig. 8). As shown in Fig. 9, targets are enclosed by agents.

V. Conclusion and Future works

This paper, as part 1, introduced a novel target-enclosing control method for PDE-based multi-agent systems, focusing on multi-step boundary control for dynamic targets in 3D space. Using backstepping control for boundary agents as leaders, we addressed these challenges in a distributed manner, laying the foundation for encirclement in part 2.

Our future work on target-enclosing will streamline the process by merging three steps into one and optimizing Step 1 to guide agents directly toward targets. We also plan to develop methods for handling dynamic target spheres, including equipping agents with estimators to assess the dynamic geometric center and radius.

References

[1] K.-K. Oh, M.-C. Park, and H.-S. Ahn, "A survey of multi-agent formation control," *Automatica*, vol. 53, pp. 424–440, 2015.

[2] P. Tabuada, G. J. Pappas, and P. Lima, "Feasible formations of multi-agent systems," in *Proceedings of the 2001 American Control Conference.(Cat. No. 01CH37148)*, vol. 1. IEEE, 2001, pp. 56–61.

[3] F. Xiao, L. Wang, J. Chen, and Y. Gao, "Finite-time formation control for multi-agent systems," *Automatica*, vol. 45, no. 11, pp. 2605–2611, 2009.

[4] L. Han, X. Dong, Q. Li, and Z. Ren, "Formation tracking control for time-delayed multi-agent systems with second-order dynamics," *Chinese Journal of Aeronautics*, vol. 30, no. 1, pp. 348–357, 2017.

[5] H. Yang and D. Ye, "Time-varying formation tracking control for high-order nonlinear multi-agent systems in fixed-time framework," *Applied Mathematics and Computation*, vol. 377, p. 125119, 2020.

[6] C. Canuto, F. Fagnani, and P. Tilli, "A Eulerian approach to the analysis of rendez-vous algorithms," *IFAC Proceedings Volumes*, vol. 41, no. 2, pp. 9039–9044, 2008.

[7] P. Frihauf and M. Krstic, "Leader-enabled deployment onto planar curves: A PDE-based approach," *IEEE Transactions on Automatic Control*, vol. 56, no. 8, pp. 1791–1806, 2010.

[8] M. Hasanzadeh and S.-X. Tang, "Dynamic average consensus as distributed pde-based control for multi-agent systems," in *2024 European Control Conference (ECC)*. IEEE, 2024, pp. 828–833.

[9] J. Qi, S.-X. Tang, and C. Wang, "Parabolic PDE-based multi-agent formation control on a cylindrical surface," *International Journal of Control*, vol. 92, no. 1, pp. 77–99, 2019.

[10] J. Zhang, R. Vazquez, J. Qi, and M. Krstic, "Multi-agent deployment in 3-D via reaction–diffusion system with radially-varying reaction," *Automatica*, vol. 161, p. 111491, 2024.

[11] Y. Shi, R. Li, and K. L. Teo, "Cooperative enclosing control for multiple moving targets by a group of agents," *International Journal of Control*, vol. 88, no. 1, pp. 80–89, 2015.

[12] S. Hara, T.-H. Kim, and Y. Hori, "Distributed formation control for target-enclosing operation by multiple dynamic agents based on a cyclic pursuit strategy," *Technical Reports, The University of Tokyo, METR*, pp. 2007–62, 2007.

[13] Y. Shi, R. Li, and T. Wei, "Target-enclosing control for second-order multi-agent systems," *International Journal of Systems Science*, vol. 46, no. 12, pp. 2279–2286, 2015.

[14] M. Hasanzadeh and S.-X. Tang, "Distributed dynamic encirclement control for first-order multi-agent systems with communication delay," in *2024 American Control Conference (ACC)*. IEEE, 2024, pp. 1000–1005.

[15] M. Hasanzadeh, M. Baradarannia, and F. Hashemzadeh, "Distributed fixed-time rotating encirclement control of linear multi-agent systems with moving targets," *Journal of the Franklin Institute*, p. 106970, 2024.

[16] M. Hasanzadeh and S.-X. Tang, "Encirclement control for PDE-based leader-follower multi-agent systems with targets in a sphere: Part 2 - rotation encirclement," *IEEE Conference on Decision and Control*, 2024.

[17] M. Krstic and A. Smyshlyaev, *Boundary control of PDEs: A course on backstepping designs*. SIAM, 2008.

[18] M. Hasanzadeh and S.-X. Tang, "Enclosing.mp4," 2024, https://www.dropbox.com/scl/fi/kpinh0in69n8abz7oynks/Enclosing.mp4?rlkey=gyno525mtv2uahzf602wrgti4&dl=0.

Authorized licensed use limited to: Texas Tech University. Downloaded on March 19,2025 at 18:55:59 UTC from IEEE Xplore. Restrictions apply.